IEEE Access
Multidisciplinary | Rapid Review | Open Access Journal

Received December 4, 2019, accepted December 29, 2019, date of publication January 3, 2020, date of current version January 10, 2020.

Digital Object Identifier 10.1109/ACCESS.2019.2963710

Reconfigurable Filter for Bandpass-to-Absorptive Bandstop Responses

TAE-HAK LEE[1], (Member, IEEE), JEAN-JACQUES LAURIN[2], (Senior Member, IEEE), AND KE WU[2], (Fellow, IEEE)

[1]Satellite Payload Research and Development Division, Korea Aerospace Research Institute, Daejeon 34133, South Korea
[2]Poly-Grames Research Center, Ecole Polytechnique, University of Montreal, Montreal, QC H3T 1J4, Canada

Corresponding author: Tae-Hak Lee (taehaklee@gmail.com)

This work was supported in part by the MDA, Thales Canada, Consortium for Research and Innovation in Aerospace in Quebec (CRIAQ), and Consortium for Aerospace Research and Innovation in Canada (CARIC).

ABSTRACT A frequency tunable filter with a bandpass-to-absorptive bandstop reconfigurable characteristic is studied, designed and validated theoretically and experimentally. To control the filter bandwidth and impedance matching performance, variable capacitors are used in each external and internal coupling structure, and, by using equivalent circuits, the required frequency responses of two different modes are obtained. Two single-pole double-throw switches embedded in the transmission lines running from the source to the load accommodate external coupling structures to control the operational mode of the proposed filter. All commercially available electronics such as switches and varactor diodes are placed on the microstrip line layer, and the frequency-tunable substrate integrated waveguide (SIW) resonators are coupled to the transmission line through coupling slots. In the absorptive bandstop mode, the stopband is tuned from 1.83 GHz to 2.49 GHz, while the passband can be tuned from 1.86 GHz to 3.3 GHz in the bandpass mode. In both modes, more than 10 dB in return loss over the frequency tuning range of interest has been achieved. Theoretical, simulated, and measured results are in good agreement, which validate the proposed filter structure.

INDEX TERMS Reconfigurable, absorptive bandstop filter, bandpass filter, single-pole double throw switch, substrate integrated waveguide (SIW) resonator.

I. INTRODUCTION

The development of reconfigurable components for wireless communication and sensing systems is of high interest to many practitioners and researchers in the field of applied electromagnetics. Reconfigurable components are developed to feature more functionalities than their conventional counterparts and can result in reduced system complexity. A significant amount of research outcomes has been reported in connection with the combination of filtering operations with other distinctive functions such as signal power division, switching and radiation [1]–[4]. RF and microwave filters, which generally consist of electrically bulky coupled resonators, still play an essential role in the development of communication systems. A reconfigurability studied and demonstrated consists of frequency-agility or switching between circuit functions, such as bandpass or bandstop as well as bandwidth tuning [5]–[14]. Two single-pole double-throw (SPDT) switches are implemented to achieve a bandstop-to-bandpass reconfigurable characteristic as shown in [5]. However, many varactor diodes are needed in the circuit chain to control resonant frequencies and coupling coefficients, and each resonator requires a switch to route the signal path. This increases design complexity significantly when such filters are designed to have higher-order responses. On the other hand, microstrip line structures have been widely used for the realization of bandpass-to-bandstop reconfigurable characteristics [6]–[10]. Most of them adopt varactor diodes to change the resonant frequency of microstrip line by adjusting its effective electrical length. However, it is not adequate for this topology to achieve wideband tuning range. Often, the structure requires more electronics for further bandwidth control. Using a substrate integrated waveguide (SIW) type of resonator, the frequency agility free from electronics has been achieved by means of a highly loaded capacitance structure [11]. With much less impact on the insertion loss, the frequency-tunable SIW resonator can tune its resonant frequency using external devices such as piezo disks or tiny motors. In [12] and [13], bandpass filters (BPFs) are studied and designed to be able to control the attenuation slope by changing the signal routes in an array of the frequency-tunable SIW resonators. However, those filters are

The associate editor coordinating the review of this manuscript and approving it for publication was Xiu Yin Zhang.

This work is licensed under a Creative Commons Attribution 4.0 License. For more information, see http://creativecommons.org/licenses/by/4.0/

limited to a bandpass response and cannot achieve multiple circuit functionalities. More operational modes of the filter such as bandpass, bandstop and all-pass modes are all studied and realized using a third-order filter structure, which does not contain coupling-tunable structure. It therefore has a limited performance in bandwidth tuning [14].

In addition to the much studied reconfigurable filter development, research aiming to reduce the reflection coefficient over the stopband of filters is of high interest [15]–[19]. In [15], bandstop filters with microstrip resonators are designed to exhibit an absorptive response in their stopband by introducing an additional destructive signal path. One-port lossy networks designed to attenuate the reflected signals from an ideal bandpass filter are used to achieve the absorptive response using lumped or distributed elements [16], [17]. By using high Q-factor SIW resonators, an absorptive bandstop filter has been demonstrated in [18], [19]. It was theoretically shown that the absorptive response can be achieved with SIW resonators by changing their Q-factor [18]. Based on a relationship of the denormalized coupling coefficients, a frequency-tunable absorptive bandstop filter with a high-Q resonator was developed in [19]. In addition, [20] presented a prototype of the absorptive bandstop-to-bandpass reconfigurable filter using microstrip ring resonators, but does not allow the control of bandwidth or operating frequency.

In [21], a reconfigurable BPF with wide frequency tuning range was proposed. Varactor diodes at each input and output port are utilized to tune the external coupling coefficients and to provide impedance matching performance over the wide frequency tuning range. In this paper, we extend and investigate the reconfigurable filter design presented in [21] by introducing a tunable characteristic to the inter-resonator coupling structure. So, the newly proposed reconfigurable filter is able to tune its bandwidth over the wide frequency tuning range. Specifically, two SPDT switches embedded in the feedline can convert the operational mode of the proposed filter between bandstop and bandpass, and variable capacitors at each external and internal coupling structure are deployed to tune the filtering bandwidth. In addition to the bandpass and absorptive bandstop responses, the proposed filter can be switched on and off by changing a bias voltage linked to the varactor diodes. Overall, the proposed reconfigurable filter achieves two functionalities: bandpass and absorptive bandstop responses. Together with a set of frequency-tunable SIW resonators, the proposed filter can also manifest a frequency agility. The bandwidth and impedance matching performance are controlled by the varactor diodes. The effect of non-ideal characteristics of the electronics on insertion loss of the prototyped filter is also investigated.

II. FILTER DESIGN

Fig. 1 shows the coupling routing diagram of the proposed reconfigurable filter and its simplified circuit schematics. S and L represent the source and load; 1 and 2 denote the tunable resonators; and SW1 and SW2 stand for SPDT switches. The two switches are set to change the switching circuit state

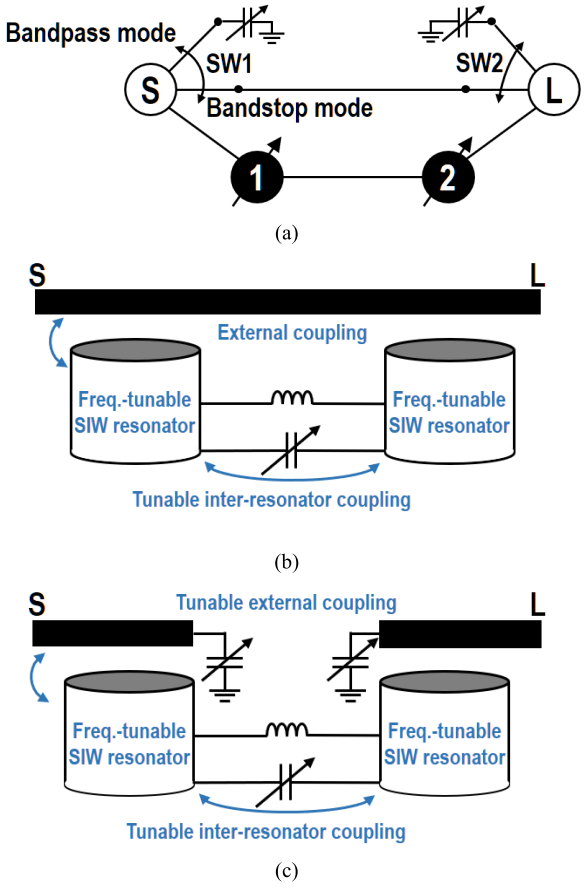

FIGURE 1. (a) Coupling routing diagram of the proposed reconfigurable filter with embedded SPDT switches, (b) simplified circuit schematic of absorptive bandstop mode, and (c) bandpass mode.

simultaneously and are always in the same state. Depending on the states of the switches, the proposed filter exhibits an absorptive bandstop or bandpass response. For the absorptive bandstop mode, the switches provide a direct path between the source and load, while these two nodes are isolated and shunt connected to the ground with varactors for the tunable bandpass mode.

The simplified circuit schematics for both operational modes are described in Figs. 1(b) and 1(c). The proposed reconfigurable filter consists of two frequency-tunable SIW resonators coupled with each other through a tunable internal coupling structure and coupled to the external transmission line. In the case of the absorptive bandstop mode, the external coupling structure is in a static state while it can be tuned using varactor diodes in the bandpass mode.

The tunable inter-resonator coupling structure is modeled using a parallel connection of LC components. The inductor will be realized in this work with a low-loss static iris coupling geometry and the tunable capacitor represents the additional coupling path that will be achieved with a microstrip line loaded with varactor diodes. The external coupling structure is realized through a coupling slot etched on top of each resonator. For the absorptive bandpass response, it is not tunable once the size is fixed at the center frequency of the

tuning range. In the bandpass mode, the tunable capacitors placed at the end of the transmission lines in Fig. 1(c) can control the external coupling coefficient for a better impedance matching performance over the frequency tuning range of interest.

The theoretical frequency responses of the two modes, namely absorptive bandstop and bandpass, can be obtained using a coupling matrix given in (1).

$$\begin{bmatrix} 0 & M_{s1} & 0 & M_{sl} \\ M_{s1} & -j\dfrac{1}{\mathrm{Q_u}\Delta} & M_{12} & 0 \\ 0 & M_{21} & -j\dfrac{1}{\mathrm{Q_u}\Delta} & M_{2l} \\ M_{sl} & 0 & M_{2l} & 0 \end{bmatrix} \tag{1}$$

where parameters $\mathrm{Q_u}$ and Δ represent the unloaded quality factor of the resonator and the fractional bandwidth of the filter, respectively. Subscripts s, l, 1 and 2 stand for the source, load and two resonators, respectively. It should be noted that two of the coupling matrix diagonal terms are related to the unloaded quality factor and the fractional bandwidth of the filter to account for the effect of Q-factor on the filter responses. Due to the symmetry of the structure in this case, the coupling coefficients M_{21} and $M_{2\,l}$ are equal to M_{12} and M_{s1}, respectively. Using (1), the S-parameters of the absorptive bandstop mode can be expressed in (2), as shown at the bottom of this page. The normalized frequency variable, s, is used and equal to $j\omega$ where ω is the radian frequency. The denominator of the diagonal coefficients in (1), $\mathrm{Q_u}\Delta$, is substituted by α in (2).

With the tunable internal coupling structure, the proposed reconfigurable filter can exhibit absorptive bandstop responses with the following coupling coefficient relationship.

$$\begin{aligned} &M_{s1}\,(=M_{2l}) = \text{arbitrary values} \\ &M_{12}\,(=M_{21}) = M_{s1}^2/2 \\ &M_{sl} = 1 \\ &\Delta = 2/Q_u M_{s1}^2 \end{aligned} \tag{3}$$

The normalized coupling coefficients can be denormalized using fractional bandwidth as follows:

$$\begin{aligned} k_{s1\mathrm{bs}} &= M_{s1}\sqrt{\Delta/2} \\ k_{12} &= M_{12}\Delta \end{aligned} \tag{4}$$

It can be noted that the relationship between external and internal coupling coefficient given in (3) is identical to the one given in [18]. However, the tunable inter-resonator coupling structure adopted in this work can effectively change the value of Δ. It results in the absorptive bandstop response, with the Q-factor which can be adjusted in the fabrication process.

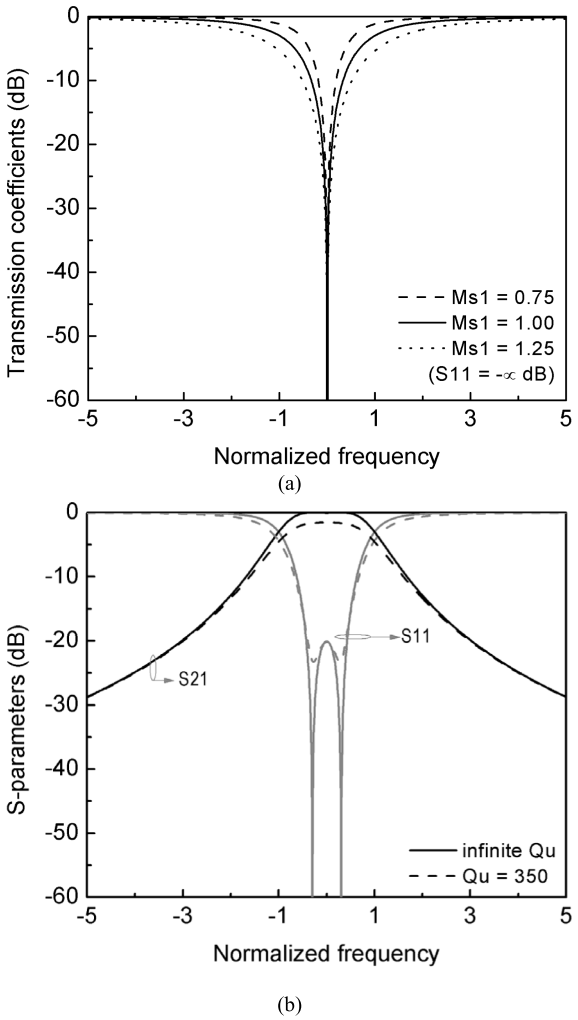

FIGURE 2. Theoretical frequency responses: (a) absorptive bandstop mode and (b) bandpass mode.

The theoretical absorptive bandstop responses are shown in Fig. 2(a) with many values for the normalized external coupling coefficient. The stopband bandwidth decreases with a smaller value of the external coupling coefficients since the required value for the inter-resonator coupling in using (3) gets also decreased. It should be noted that the magnitude of the reflection coefficient is theoretically zero regardless of the external coupling coefficient.

$$\begin{aligned} |S_{21}(\omega)| &= \frac{2i\left(\alpha^2 s^2 + 2\alpha s + M_{12}^2\alpha^2 - M_{12}M_{s1}^2\alpha^2 + 1\right)}{2\alpha^2 s^2 + \left(4\alpha + 2M_{s1}^2\alpha^2\right)s + \left(M_{s1}^4\alpha^2 + 2M_{12}^2\alpha^2 - 2M_{12}M_{s1}^2\alpha^2 + 2M_{s1}^2\alpha + 2\right)} \\ |S_{11}(\omega)| &= 1 - \frac{2\left(\alpha^2 s^2 + \left(M_{s1}^2\alpha^2 + 2\alpha\right) + M_{12}^2\alpha^2 + M_{s1}^2\alpha + 1\right)}{2\alpha^2 s^2 + \left(4\alpha + 2M_{s1}^2\alpha^2\right)s + \left(M_{s1}^4\alpha^2 + 2M_{12}^2\alpha^2 - 2M_{12}M_{s1}^2\alpha^2 + 2M_{s1}^2\alpha + 2\right)} \end{aligned} \tag{2}$$

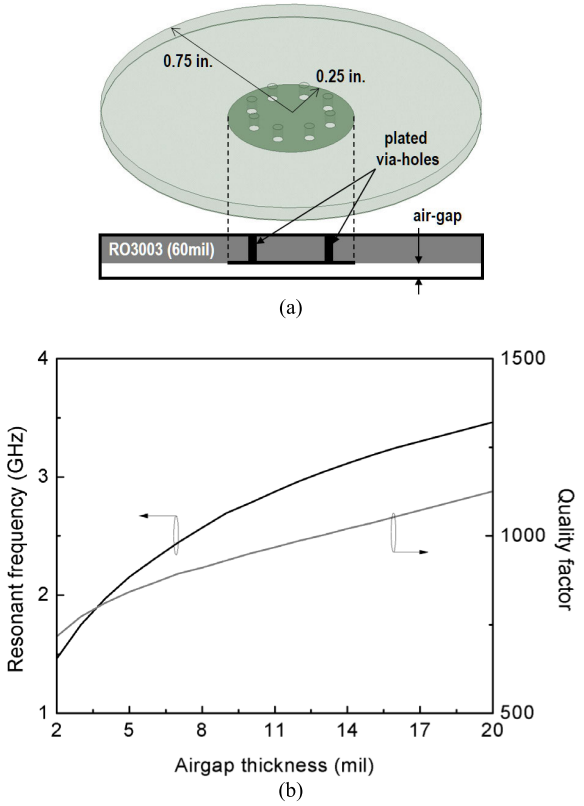

FIGURE 3. (a) SIW resonator for eigen-mode simulation and (b) its results of resonant frequency and quality factor.

For the bandpass mode, the proposed reconfigurable filter is designed to exhibit the classical second order bandpass response, as shown in Fig. 2(b). M_{s1} ($= M_{2l}$), M_{12} ($= M_{21}$), and M_{sl} are 0.8010, 0.7087 and 0, respectively. To investigate the effect of the unloaded Q factor of the resonator on the bandpass response, an arbitrarily chosen Q_u-value of 350 is applied with a fractional bandwidth of 0.023. This can result in about 1.5 dB of insertion loss. In the following section, we describe the detailed structure of the frequency-tunable SIW resonator and its coupling structures for external and inter-resonator couplings.

A. COUPLING STRUCTURES

Prior to the design of coupling structures with frequency-tunable SIW resonators, the characteristics of resonator, such as resonant frequency and quality factor, have been simulated and examined. As shown in Fig. 3(a), a circular shaped cavity filled with two layers of dielectrics (air and RO3003 material from Rogers) is used to model the SIW resonator for simplicity. A circular disk, which will be used in this work to realize a tunable capacitor, is printed at the interface of the two dielectrics. The disk is connected to the upper cavity wall with eight plated vias to ensure the Q-factor and connection to the ground. The first resonant mode of the resonator is mainly determined by the capacitance between the circular disk and the bottom cavity wall, and it can be accurately tuned by changing the thickness of the air layer. The simulated

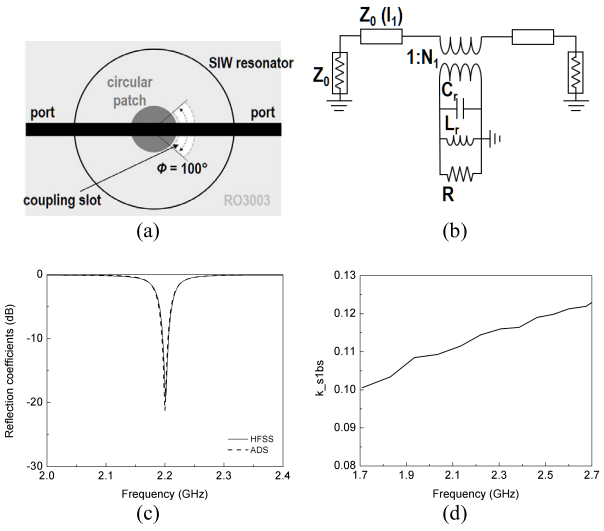

FIGURE 4. (a) Simplified circuit schematic for the external coupling of bandstop mode, (b) equivalent circuit, (c) simulation results of reflection coefficients, and (d) calculated k_{s1bs}s with frequency changes.

resonant frequency and the Q-factor are given in Fig. 3(b). Simulations were carried out with the 3D eigenmode solver of ANSYS-HFSS. The slope of these two responses can be controlled with the ratio of the cavity and disk radii. Therefore, the dimensions for the cavity and patch can be determined as to achieve the resonant frequency changes of interest and the high quality factor values with a reasonable air-gap thickness variation [22].

Fig. 4(a) shows the external coupling structure of the absorptive bandstop mode. A second dielectric substrate (Rogers3003 with $\varepsilon_r = 3$ and thickness $= 20$ mils) is added on the top of the cavity to support the microstrip line. Each end of the transmission line is connected to the source and load, and an arc-shaped coupling slot etched on top of the resonator is used to form a magnetic coupling between the line and resonator. The arc length is 100 degrees, and the width of the slot is 50 mils to achieve the required external coupling coefficient value at 2.2 GHz, as shown in Fig. 4(c). An equivalent circuit consisting of the LC components with a transformer can model the external coupling structure. The simulated reflection coefficient results obtained with two different simulation tools, the ANSYS HFSS and Keysight ADS, show a good agreement with C_r'$= 50$ pF, the turning ratio of $N_1 = 1.05$ at the center frequency of 2.2 GHz of the absorptive bandstop mode. It should be noted that a parallel resistor ($R = Q_u/(\omega_0 C_r)$) representing the Q-factor given in Fig. 3(b) is added to emulate the simulation results obtained from HFSS. The relatively short microstrip lines ($l_1 = \lambda_g/60$) are placed at both ends of the transformer. The calculated k_{s1bs} values are plotted in Fig. 4(d), showing a monotonic increase with frequency.

Fig. 5 shows the simplified internal couplings structure and its equivalent circuit representing two different paths for the internal coupling, the iris and varactor-loaded microstrip line. In order to achieve a tunable characteristic, two different

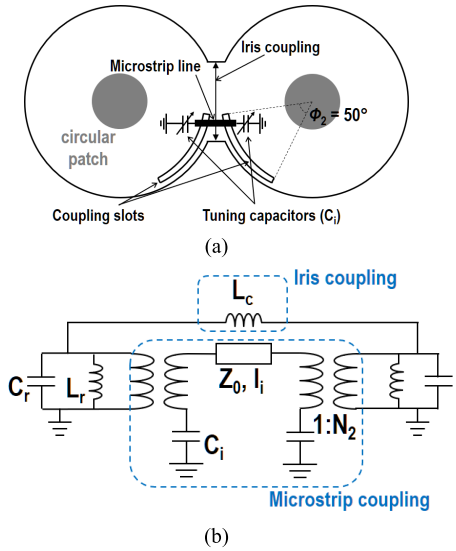

FIGURE 5. (a) Simplified model for tunable inter-resonator coupling structure and (b) equivalent circuit.

coupling paths are introduced in the internal coupling structure. One is a static, low-loss iris coupling path which can be modeled using one series inductor, L_c $(= L_r/(M_{12}\Delta))$, as shown in Fig. 5(b). The other is a varactor-loaded microstrip line coupled through an additional arc-shaped slot etched on top of the resonator. It is designed to be tunable with two capacitors C_i and a microstrip line whose length and impedance are equal to l_i and Z_0, respectively. The coupling between the varactor diodes loaded microstrip line and the resonator is modeled using a transformer with a turn ratio of 2.2 during the circuit simulation. In addition, the microstrip line is set to have the length of 5 mm in considering the dimensions of the SIW resonators. It should be noted that, in the absorptive bandstop mode, the tunable characteristic of the internal coupling structure can compensate for the deviation of the coupling coefficients resulting from the changing resonant frequency over the tuning range, as shown in the calculated results in Fig. 4(d).

Internal coupling structures implemented with either or both series inductor and microstrip line with tunable capacitors were simulated, and the results from ADS and HFSS are given in Fig. 6. The equivalent circuits are simulated at the lower and higher ends of the tuning range of the bandpass mode, and the values of k_{12} are calculated using the results obtained from HFSS. It should be noted that both modes of the proposed reconfigurable filter share the internal coupling structure shown in Fig. 5. For the k_{12} results given in Fig. 6(c), the range of the capacitance value is selected based on a commercial varactor diodes datasheet.

The frequency responses of the equivalent circuit having only a static inductor, L_c, for internal coupling are shown in gray lines. Since the internal coupling structure is symmetrical, it can be interpreted using an even- and odd-mode analysis. The even mode frequency, f_e, is determined using

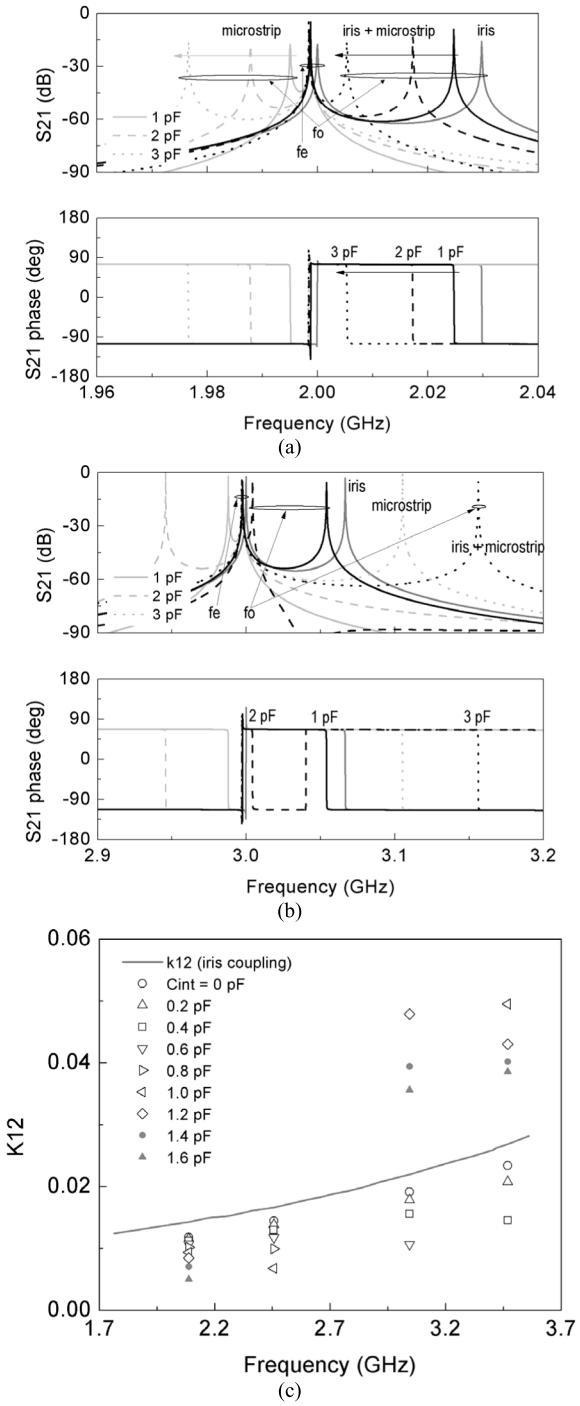

FIGURE 6. Simulated results of the tunable inter-resonator coupling structure: (a) $f_e = 2$ GHz, (b) $f_e = 3$ GHz, and (c) HFSS results.

$1/(2\pi L_r C_r)$, where the LC values are the same as in Fig. 4(b). On the other hand, the odd mode frequency, f_o, is placed higher than f_e as half of L_c is connected to L_r in parallel. It results in the phase characteristic whose positive 90° response is between two resonant peaks [23]. The responses obtained from the equivalent circuit having only the microstrip line with tunable capacitors, C_i, are also given

in Figs. 6(a) and 6(b). The shunt-connected variable capacitor generates f_o lower than f_e, so the opposite phase characteristic is obtained when a L_c is used for the internal coupling. Larger capacitance loading causes lower odd mode frequency and results in larger k_{12} values according to (5).

$$k_{12} = \left| \frac{f_e^2 - f_o^2}{f_e^2 + f_o^2} \right| \tag{5}$$

The simulation results of the equivalent circuit which possess both coupling structures are also given in Figs. 6(a) and 6(b). As the larger capacitance is applied, the two resonant peaks come closer, resulting in small k_{12} values. The scalar summation of k_{12} obtained from the two aforementioned different coupling structures can be used as an approximation of k_{12} when the circuit has both coupling structures [13].

$$k_{12iris} + k_{12microstrip} \approx k_{12tot} \tag{6}$$

It should be noted that the coupling between the resonator and the microstrip line for the internal coupling is tightened over the higher frequency band. In other words, with the same amount of C_i loading variation, the larger value and variation of k_{12} can be obtained at 3 GHz, as shown in Fig. 6(c). In addition, the electrical length of the microstrip line is no longer negligible with the increased resonant frequency, and an additional odd mode resonance is generated as in the previously reported works [12], [13]. It can be concluded that the internal coupling structure which has two paths (one for the iris and the other for the capacitor loaded microstrip) can provide a set of variable k_{12} values by changing the value of C_i.

In Fig. 6(c), the simulated results of the tunable inter-resonator coupling structure using HFSS are given. The length of the microstrip line is mostly dependent on the diameter of the resonator. The size of the additional coupling slot for internal coupling is optimized by taking into account the capacitance values from commercially available varactor diodes. The solid black line represents the calculated k_{12} values when two resonators are coupled with one another using only the iris structure while the symbols show the calculated k_{12} values with loaded capacitance. The simulated and calculated results are given at 2, 2.5, 3 and 3.5 GHz.

Based on the aforementioned external and internal coupling structures, the equivalent circuit shown in Fig. 7(a) can generate the frequency responses of the absorptive bandstop mode. The values of lumped elements calculated for the external and internal coupling structure can be applied to the filter structure. In addition to the two coupling structures, a transmission line whose electrical length is an odd multiple of the quarter wavelength at the center frequency is added to provide a direct coupling between the two ports. Fig. 7(b) shows the simulated absorptive bandstop response over the frequency tuning range of interest. The theoretical responses are obtained from the coupling coefficients in (3) with an

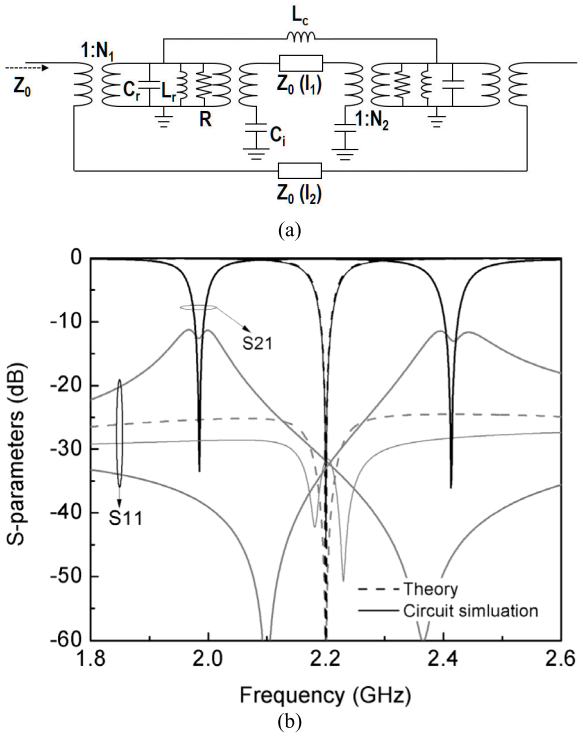

FIGURE 7. (a) Equivalent circuit for absorptive bandstop mode and (b) simulated S-parameters.

arbitrarily chosen value of $M_{s1} = 1$ and a fractional bandwidth of $\Delta = 0.025$. While considering the operation mechanism of the frequency-tunable SIW resonator shown in Fig. 3(a), the capacitance used to model the resonator, C_r, is changed to tune the operating frequency during the simulation. Due to the frequency dependent characteristic of the microstrip line, the reflection coefficient is changed over the tuning range. In order to keep the absorptive characteristic, the capacitance value for inter-resonator coupling, C_i, is tuned from 0.3 pF to 1.3 pF. It can be seen that the absorptive bandstop responses can be tuned between 2 and 2.4 GHz approximately, with less than -10 dB reflection coefficients. With a consideration of circuit complexity and additional losses from electronics, the absorptive bandstop mode is designed to have a fixed stopband bandwidth.

For the bandpass mode, the proposed reconfigurable filter is designed to achieve a tunable external coupling characteristic by embedding the SPDT switches into the transmission line as shown in Fig. 1(c). Fig. 8(a) shows a simplified tunable external coupling structure in the bandpass mode. In [9], a single-pole double-throw (SPST) switch embedded in the microstrip line is used for switching the operational mode, so the placement of the switch and its electrical length, when it is turned off, can determine the external coupling. In this work, the SPDT switch can provide more freedom to design the external coupling structure for the bandpass mode, even if the size of a coupling slot etched on the resonator is determined in the previous design process.

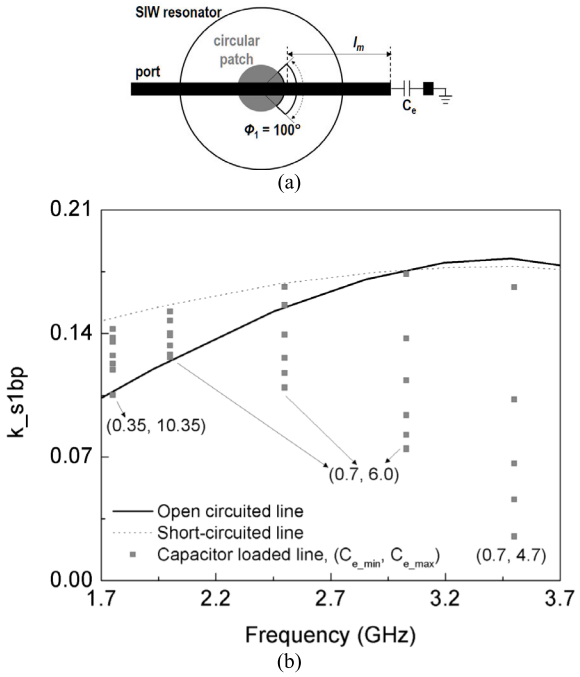

FIGURE 8. (a) Simplified model for external coupling of bandpass mode and (b) simulated results.

In Fig. 8(b), three different external coupling structures are compared to show the advantage of using the SPDT switches over the previous designs. The solid or dotted lines show the external coupling coefficient variations over the frequency tuning range without C_e loading. The electrical length of the line is set to be zero for the short circuited line and one quarter wavelength at 3.3 GHz for the open circuit line. The electrical length of the microstrip line for the open circuited case is set to have a maximum field intensity at the coupling slot, which results in a large external coupling coefficient k_{s1bp}.

In addition, the tunable external characteristic can be obtained by adding a variable capacitor, C_e, in the microstrip line as shown in Fig. 8(b). In this case, the tunable external coupling structure of the bandpass mode can be used to control the impedance matching characteristics over the frequency tuning range, even if the bandwidth changes.

Fig. 9 shows the equivalent circuit of the bandpass mode and its simulated circuit performance related to the resonant frequency and bandwidth tuning. The capacitance value for each resonator, C_r, is tuned to change the resonant frequency from around 1.85 GHz to 3.3 GHz, and the simulated results show that the bandwidth has been changed from around 40 MHz to 100 MHz over the wide frequency tuning range. The 3 dB bandwidth is mainly tuned with the variation of C_i, and the reflection coefficient in the passband is maintained below -10 dB by tuning the value of C_e, as shown in Fig. 9(c). It should be noted that the bandwidth is changed from 26 MHz to 52 MHz with the variation of C_i value from 1.25 pF to 0.2 pF. It is consistent with the simulation results given in Fig. 6(c).

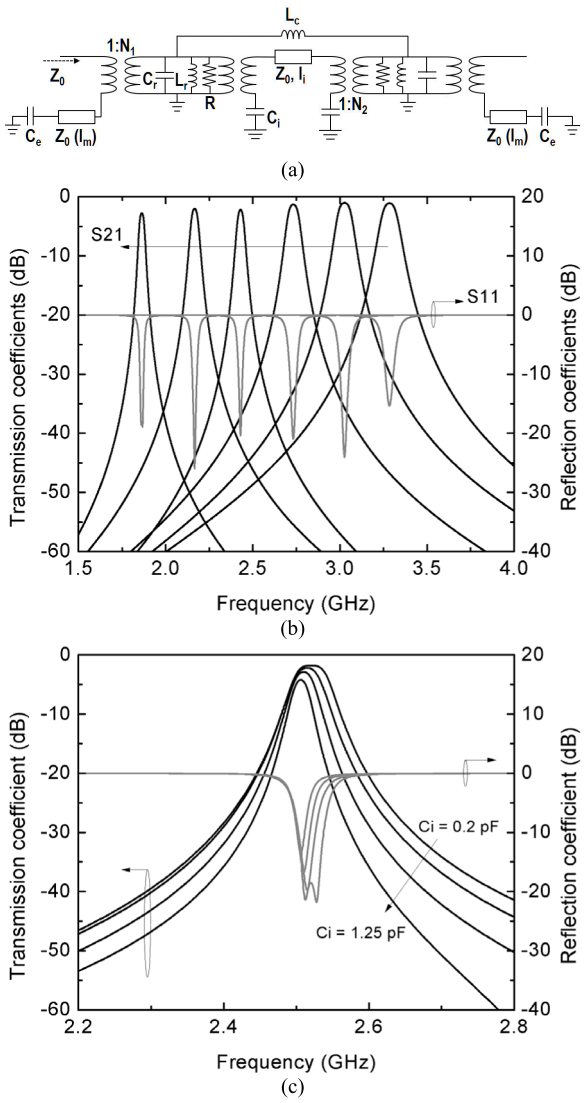

FIGURE 9. (a) Equivalent circuit for bandpass mode, (b) simulated results of resonant frequency tuning and (c) simulated results with different capacitance loading for C_i for bandwidth tuning.

B. SPDT SWITCH CHARACTERIZATION

As mentioned in the previous sections, two SPDT switches are embedded in the transmission line of the proposed reconfigurable filter to switch between the bandpass and absorptive bandstop modes. In order to design the coupling structures and to satisfy the required electrical length of the microstrip line, the electrical performance of the switches needs to be investigated. Fig. 10 shows the photograph of a fabricated test-bed for a SPDT switch. An SPDT switch (SKY13330-397LF from Skyworks co.) is soldered on the substrate (20 mil-thick RO3003 from Rogers co.). Its frequency response is measured as given in Fig. 10(b). The measured results show that one switch can provide around 0.35 dB insertion loss over the frequency tuning range of interest, from 1.5 GHz to 3.5 GHz, with less than −20 dB of reflection coefficient.

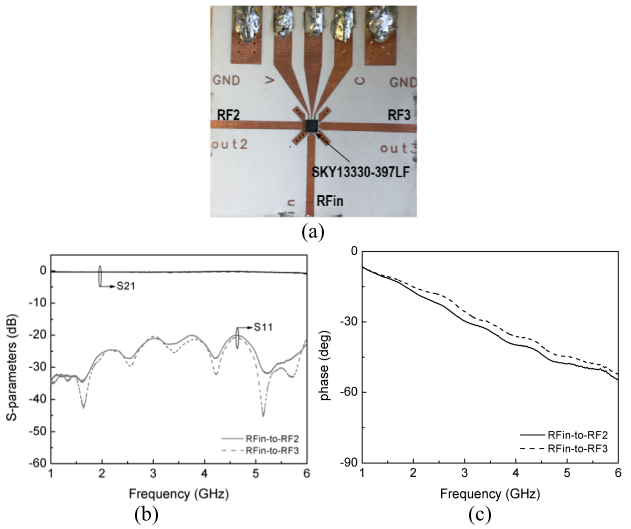

FIGURE 10. (a) Photograph of test-bed for SPDT switch, (b) measured S-parameters, and (c) transmission phase inside the switch.

It is important to measure the phase shift introduced by the switch since it can increase the electrical length of the microstrip line, l_m, of the external coupling structure of the bandpass mode. It can also contribute to the electrical length of the microstrip line between two coupling slots, namely l_2 of Fig. 7(a), which need to be an odd multiple of one quarter wavelength for the absorptive bandstop mode. The phase of the transmission coefficient can be computed by comparing the measured phase response of the fabricated test-bed without the switch to the scenario with the switch. The calculated results are shown in Fig. 10(c). The measured phase result is used to determine the length of the microstrip line l_m of Fig. 8(a) during the simulation of the external coupling structure of the bandpass mode.

III. EXPERIMENTAL VALIDATION

The proposed bandpass-to-absorptive bandstop reconfigurable filter has been fabricated and measured to support the aforementioned design theory. The 60 mil- and 5 mil-thick substrates are used for the development of the frequency-tunable SIW resonator, and the microstrip line structure is etched on the 20mil-thick substrate. All substrates are of the same type, namely RO3003 ($\varepsilon_r = 3.0$, $\tan\delta = 0.001$) from Rogers Corporation. The alignment between the resonators, microstrip line, and coupling slots is shown in Fig. 11(a). Figs. 11(b), 11(c), and 11(d) respectively show the photographs of the microstrip line, copper membrane layers of the fabricated filter, and its simplified cross section view along the gray dotted line of Fig. 11(c) with two external frequency tuning elements. All the electronic parts such as SPDT switches, varactor diodes, and lumped elements for biasing are soldered onto the microstrip line. It should be noted that the two varactor diodes are connected back-to-back to provide a precise capacitance control with no additional DC-block capacitor. As shown in the

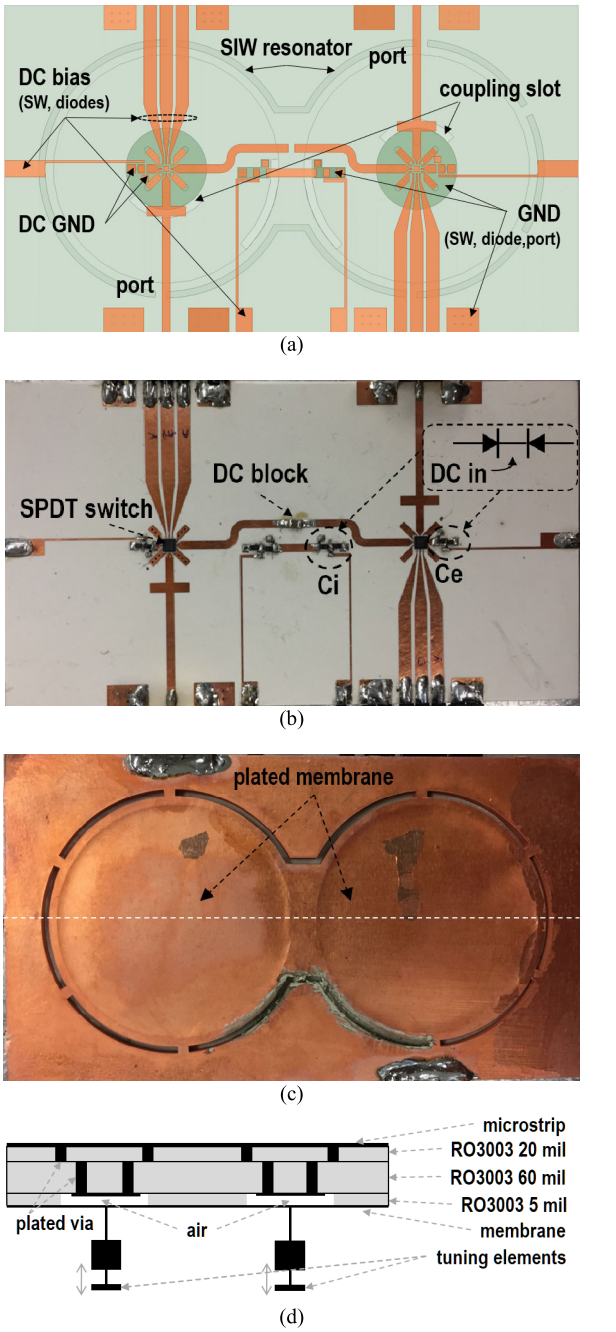

FIGURE 11. (a) Proposed reconfigurable filter configuration, (b) photograph of microstrip line layer, (c) photograph of membrane layer of the fabricated filter, and (d) simplified cross-section view with external frequency tuning elements.

simulation results given in Figs. 6(c) and 8(b), small changes in capacitance can lead to a large amount of coupling coefficients in the higher frequency band. For tuning the internal coupling coefficients, two varactor diodes (SMV2020 from Skyworks, 0.35∼3.2pF with bias voltage up to 20V) are loaded on each resonator. A different type of varactor diode (SMV1265-040LF from Skyworks, 0.71∼22.47pF with bias voltage up to 30V) is implemented to change

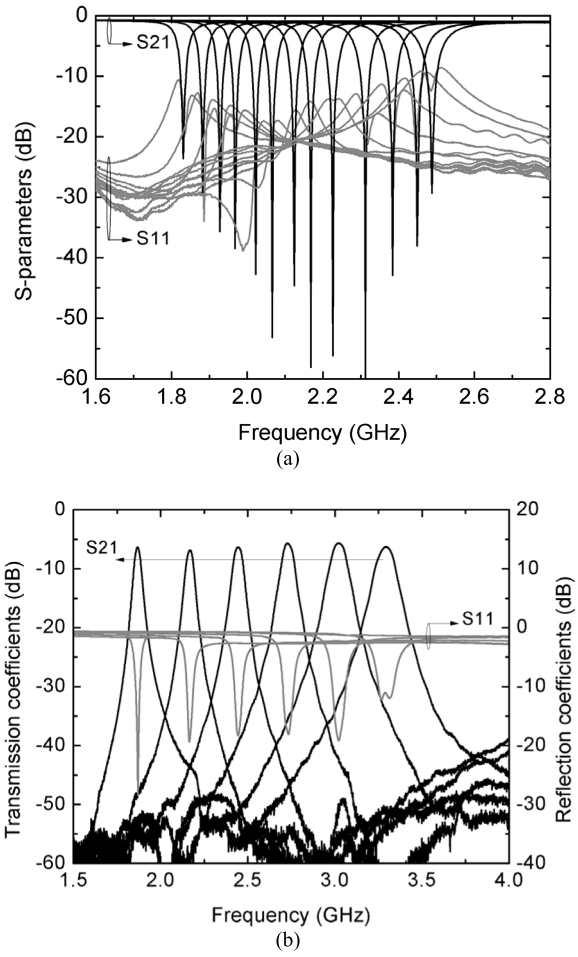

FIGURE 12. Measured S-parameter results: (a) absorptive bandstop mode and (b) bandpass mode.

the capacitance, C_e. In order to provide the appropriate RF signal route, a 100 kΩ resistor is added to the bias circuit, and a DC block capacitor (C08BL242X from Knowles dielectric Lab.) is added into the microstrip line to avoid the interaction between the two switches in the absorptive bandstop mode.

The resonant frequency of the SIW resonator can be tuned by changing the thickness of the air-gap generated by the 5 mil-thick substrate with copper foil. To ensure the electrical contact of the copper foil to the ground of the resonators, an additional plating process is performed. Two piezo-based linear actuators, which can provide deflection, in the order of one centimeter, are attached to the resonators for the frequency tuning, as shown in Fig. 11(d). Their detailed operational mechanism can be found in [24].

Fig. 12 shows the measured frequency responses of the fabricated reconfigurable filter. The absorptive bandstop mode achieves more than a 50-dB insertion loss at the operating frequency of 2.2 GHz with less than −15 dB reflection coefficient. Above and below the design frequency of 2.2 GHz,

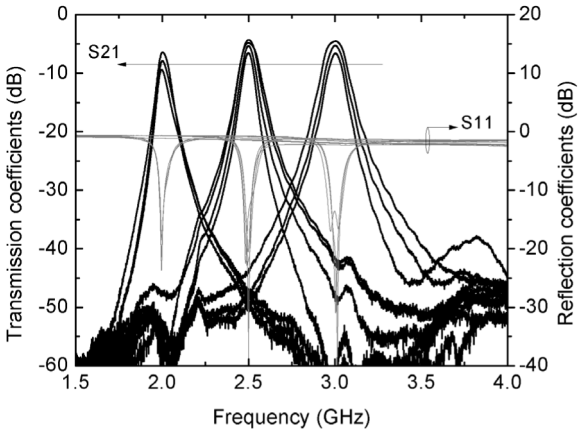

FIGURE 13. Bandwidth tuning performance of bandpass mode.

both the reflection coefficient and insertion loss are increased due to the frequency dependent characteristic of the coupling structure and microstrip line. In the absorptive bandstop mode, the measured frequency tuning range is about 680 MHz (30%) with the reflection coefficients less than −10 dB over the frequency tuning range.

The S-parameters of the bandpass mode of the fabricated filter are shown in Fig. 12(b). The passband can be continuously tuned from 1.86 GHz to 3.3 GHz with more than 10 dB in return loss and about 7 dB in insertion loss. The measurement results of the bandpass mode are given in a way to prove that the proposed reconfigurable filter can maintain its impedance matching performance over the wide frequency tuning range. It can be achieved with the tunable external and inter-resonator coupling structures.

The 3-dB bandwidth also can be tuned using the tunable inter-resonator coupling structure with varactor diodes, C_i. Fig. 13 shows the measured bandwidth tuning performance at 2.0, 2.5 and 3.0 GHz as an example. During a 3-dB bandwidth tuning, the return loss at the center frequency is also controlled in order to keep it larger than 10 dB by adjusting the bias voltage on C_e. The insertion loss increases when the filter is tuned to have the narrower bandwidth. This insertion loss characteristic is mainly dependent on the quality factors of the varactor diodes placed in the coupling structures and it can be improved with those having high Q-factor [12], [13].

Based on the bandwidth tuning characteristic of the proposed filter, the passband can be tuned in to maintain its absolute bandwidth. Fig. 14 shows two examples where the passband is tuned with the predefined bandwidths of 80 MHz and 45 MHz. More specifically, the 3-dB bandwidth changes for each case are from 79.95 MHz to 88.10 MHz and from 45.06 MHz to 49.2 MHz with the tuning range of 640 MHz and 600 MHz, respectively. It should be noted that the frequency tuning range can be limited when the filter has been tuned to achieve the constant absolute

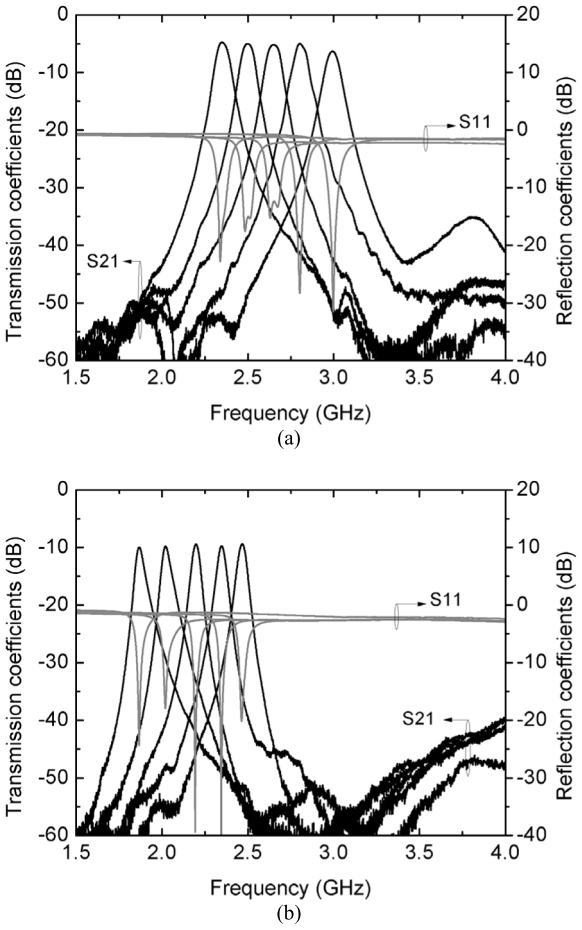

FIGURE 14. Measured S-parameters of bandpass mode with constant absolute bandwidth characteristic: (a) 80 MHz and (b) 45 MHz.

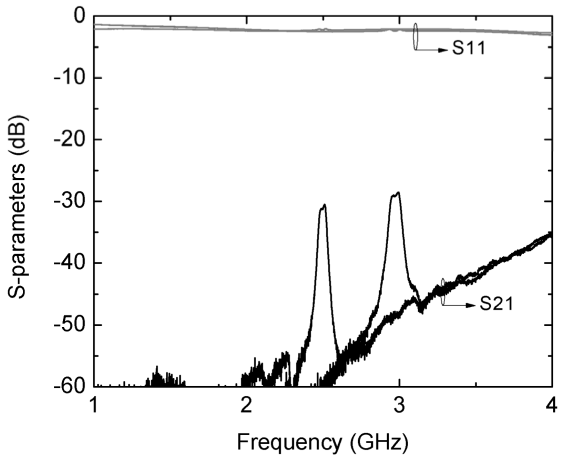

FIGURE 15. Measured S-parameters of switched-off state.

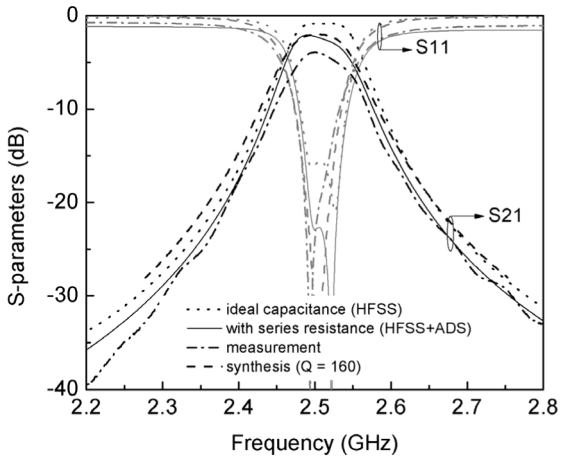

FIGURE 16. Frequency responses comparison for non-ideal effect from varactor diodes.

bandwidth characteristic. This is due to a limited tuning range of the capacitance from commercially available varactor diodes, as shown in Fig. 6(c).

In addition to the absorptive bandstop and bandpass modes, the reconfigurable filter can be switched on-off with a large amount of loaded capacitance for C_e. In other words, the fabricated filter can be instantly turned off in the bandpass mode by applying 0V to the varactor diodes in the external coupling structure. From the datasheet of the varactor diode, the typical capacitance of a 0-V varactor diode is 22.47 pF. Fig. 15 shows the measured responses of the two switched-off state. The measured return loss is less than 3.5 dB loss over the frequency tuning range of interest. It is mainly due to the series resistance of the varactor diodes.

To investigate the effect of non-ideal characteristics from the varactor diode and fabrication process, the frequency responses of the bandpass mode at 2.5 GHz are simulated and compared with the measured results, as given in Fig. 16. The simulation results obtained using the HFSS account for the losses from dielectrics and conductors, which show about 0.83 dB in insertion loss. During the simulation process, the capacitors at the external and inter-resonator coupling structures are assumed to have an ideal characteristic without resistors of the varactor diodes. Using the circuit simulation tool, the additional series resistors are added to the ideal capacitors, and they can result in additional 2.08 dB of insertion loss. It should be noted that a single 5-Ω resistor is used to model the series resistors of the back-to-back connected varactor diodes. Based on the synthesis results, the frequency response obtained with the effective Q-factor of 160, which use (2), can provide a comparable insertion loss level. The additional losses can come from the two SPDT switches which is about 0.7 dB as shown in Fig. 10(b) and from the adhesive and the silver pasts for the multilayer and SIW fabrication.

To recapitulate the proposed filter, Table 1 provides a comparison between filters which have been proposed to realize the reconfigurable characteristics. We believe that a wide tuning range of the passband and absorptive bandstop characteristics can be achieved with the proposed SIW filter design.

TABLE 1. Comparison table.

	Available response	Agility	Type of resonator	Frequency / bandwidth tuning method	Tuning range	Single resonator size	I.L. (BP mode)	Filter order
[6]	Bandpass / Bandstop	Frequency / Order / Bandwidth	Microstrip	varactor diodes	0.72~1.01 GHz / 2, 4 / 3.1~9.4%	(width × length) 1.4 × 15	< 5 dB / < 7.5 dB	4
[7]	Bandpass / Bandstop	Frequency / Bandwidth	Microstrip	varactor diodes	0.76~1.08 GHz / 6.8~12.2%	17 × 22	< 5 dB / 6.0~3.5 dB	4
[8]	Dual band Bandpass / Bandstop	Bandwidth	Microstrip	varactor diodes	4.5~24% at f_0 / 4.5~13% at f_1	Not available	< 2.4 dB / < 4.7 dB	2
[9]	Dual band Bandpass / Bandstop	Frequency	Microstrip	varactor diodes	1.7~2.2 GHz at f_0 / 2.2~2.7 GHz at f_0	Not available	< 5.0 dB / < 4.6 dB	2
[10]	Bandpass / Bandstop	Frequency	Microstrip	varactor diodes	0.95~1.35 GHz	33 × 10	< 5.6 dB	2
[5]	Bandpass / Bandstop	Frequency / Bandwidth	SIW	varactor diodes	2.15~2.75 GHz / 4.1~8.2%	(diameter × height) 5.6 × 3.175	< 7 dB / 3~6 dB	2
[12]	Bandpass	Frequency / Order	SIW	Piezo disks / varactor diodes	2.7~3.1 GHz / 2~4	15 × 3.175	< 7.6 dB	4
[14]	Bandpass / Bandstop / Allpass	Frequency	SIW	Piezo based motors / Not available	3.0~2.6 GHz	15.4 × 3.175	< 2.4 dB	3
[18]	Bandstop / Allpass	Frequency	SIW	Piezo disks	2.75~3.15 GHz	13.6 × 3.175	Not Available	2
[19]	Absorptive Bandstop	Frequency	SIW	Piezo disks / Not available	3.4~3.8 GHz	13.1 × 3.175	Not Available	2
[21]	Bandpass / Allpass	Frequency	SIW	Piezo disks / Not available	1.34~2.31 GHz	25 × 1.524	< 4.5 dB	2
This work	Bandpass / Absorptive bandstop	Frequency, Bandwidth / Frequency	SIW	Piezo based motors / varactor diodes	1.86~3.3 GHz, 2.0~3.9% / 1.83~2.48 GHz	38.1 × 1.524	< 6.7 dB / 4.8 ~ 10.0 dB	2

IV. CONCLUSION

In this paper, we introduce and investigate a frequency tunable reconfigurable filter that can switch from bandpass to absorptive bandstop responses and vice-versa. Two single-pole double-throw switches are embedded in the transmission line and used to control the operating modes of the proposed reconfigurable filter. Variable capacitors are implemented to achieve the tunable characteristics of the external and inter-resonator couplings. Using the equivalent circuits developed in this work, the proposed reconfigurable filters are analyzed and discussed in detail. The operating frequency of both modes, namely bandpass and absorptive bandstop, has been tuned as desired and the fabricated filter achieves 1:1.77 and 1:1.36 frequency tuning ratio, respectively. In addition, the proposed reconfigurable filter can also be turned on and off with the minimized external coupling coefficient. The measured results of the fabricated filter prototype have supported and validated the design theory of the proposed reconfigurable filter.

ACKNOWLEDGMENT

The authors would like to thank T. Antonescu and M. Thibault from the Poly-Grames Research Center for their special fabrication support.

REFERENCES

[1] R. Gomez-Garcia, J.-M. Munoz-Ferreras, and D. Psychogiou, "RF reflectionless filtering power dividers," *IEEE Trans. Circuits Syst. II, Exp. Briefs*, vol. 66, no. 6, pp. 933–937, Jun. 2019.

[2] J.-X. Xu, X. Y. Zhang, H.-Y. Li, and Y. Yang, "Narrowband single–pole double–throw filtering switch based on dielectric resonator," *IEEE Microw. Wireless Compon. Lett.*, vol. 28, no. 7, pp. 594–596, Jul. 2018.

[3] J.-M. Yan, H.-Y. Zhou, and L.-Z. Cao, "A novel filtering balun and improvement of its isolation performance," *IEEE Microw. Wireless Compon. Lett.*, vol. 27, no. 12, pp. 1056–1058, Dec. 2017.

[4] K. Dhwaj, L. J. Jiang, and T. Itoh, "Dual–band filtering antenna with novel transmission zero characteristics," *IEEE Antennas Wireless Propag. Lett.*, vol. 17, no. 12, pp. 2469–2473, Dec. 2018.

[5] T. Yang and G. M. Rebeiz, "Bandpass-to-bandstop reconfigurable tunable filters with frequency and bandwidth controls," *IEEE Trans. Microw. Theory Techn.*, vol. 65, no. 7, pp. 2288–2297, Jul. 2017.

[6] Y.-H. Cho and G. M. Rebeiz, "Two- and four-pole tunable 0.7–1.1-GHz bandpass-to-bandstop filters with bandwidth control," *IEEE Trans. Microw. Theory Techn.*, vol. 62, no. 3, pp. 457–463, Mar. 2014.

[7] Y.-H. Cho and G. M. Rebeiz, "0.7–1.0-GHz reconfigurable bandpass-to-bandstop filter with selectable 2- and 4-pole responses," *IEEE Trans. Microw. Theory Techn.*, vol. 62, no. 11, pp. 2626–2632, Nov. 2014.

[8] N. Kumar and Y. K. Singh, "RF-MEMS-based bandpass-to-bandstop switchable single- and dual–band filters with variable FBW and reconfigurable selectivity," *IEEE Trans. Microw. Theory Techn.*, vol. 65, no. 10, pp. 3824–3837, Oct. 2017.

[9] F.-C. Chen, R.-S. Li, and J.-P. Chen, "A tunable dual–band bandpass-to-bandstop filter using p-i-n diodes and varactors," *IEEE Access*, vol. 6, pp. 46058–46065, 2018.

[10] K. Song, W. Chen, S. R. Patience, Y. Chen, A. M. Iman, and Y. Fan, "Compact wide–frequency tunable filter with switchable bandpass and bandstop frequency response," *IEEE Access*, vol. 7, pp. 47503–47508, 2019.

[11] S. Moon, H. H. Sigmarsson, H. Joshi, and W. J. Chappell, "Substrate integrated evanescent–mode cavity filter with a 3.5 to 1 tuning ratio," *IEEE Microw. Wireless Compon. Lett.*, vol. 20, no. 8, pp. 450–452, Aug. 2010.

[12] J. Lee, E. J. Naglich, H. H. Sigmarsson, D. Peroulis, and W. J. Chappell, "Tunable inter–resonator coupling structure with positive and negative values and its application to the field–programmable filter array (FPFA)," *IEEE Trans. Microw. Theory Techn.*, vol. 59, no. 12, pp. 3389–3400, Dec. 2011.

[13] B. Koh, B. Lee, S. Nam, T.-H. Lee, and J. Lee, "Integration of interresonator coupling structures with applications to filter systems with signal route selectivity," *IEEE Trans. Microw. Theory Techn.*, vol. 64, no. 9, pp. 2790–2803, Sep. 2016.
[14] T.-H. Lee, B. Lee, S. Nam, Y.-S. Kim, and J. Lee, "Frequency–tunable tri–function filter," *IEEE Trans. Microw. Theory Techn.*, vol. 65, no. 11, pp. 4584–4592, Nov. 2017.
[15] D. R. Jachowski, "Passive enhancement of resonator Q in microwave notch filters," in *IEEE MTT-S Int. Microw. Symp. Dig.*, Jun. 2004, pp. 1315–1318.
[16] T.-H. Lee, B. Lee, Y.-S. Kim, K. Wu, and J. Lee, "Higher order lumped element absorptive low-pass and bandpass filter structures," *IET Microw., Antennas Propag.*, vol. 13, no. 8, pp. 1166–1173, Jul. 2019.
[17] S.-W. Jeong, T.-H. Lee, and J. Lee, "Absorptive filter prototype and distributed element absorptive bandpass filter," in *IEEE MTT-S Int. Microw. Symp. Dig.*, Reykjavík, Iceland, Aug. 2018, pp. 1–4.
[18] E. J. Naglich, J. Lee, D. Peroulis, and W. J. Chappell, "Switchless tunable bandstop-to-all-pass reconfigurable filter," *IEEE Trans. Microw. Theory Techn.*, vol. 60, no. 5, pp. 1258–1265, May 2012.
[19] T. Snow, J. Lee, and W. J. Chappell, "Tunable high quality-factor absorptive bandstop filter design," in *IEEE MTT-S Int. Microw. Symp. Dig.*, Jun. 2012, pp. 1–3.
[20] M. K. Zahari, B. H. Almad, W. P. Wen, and N. A. Shairi, "Switchable bandstop to bandpass filter using parallel-coupled resonator," in *Proc. IEEE Asia–Pacific Microw. Conf. (APMC)*, Nov. 2017, pp. 513–516.
[21] T.-H. Lee and K. Wu, "Bandpass-to-all-pass reconfigurable filter with wide frequency tuning range," in *IEEE Int. Wireless Symp. Dig.*, Chengdu, China, May 2018, pp. 1–4.
[22] H. Joshi, H. H. Sigmarsson, and W. J. Chappell, "Analytical modeling of highly loaded evanescent-mode cavity resonators for widely tunable high-Q filter applications," in *Proc. Union Radio Sci. Int. (URSI)*, Chicago, IL, USA, Aug. 2008, pp. 1–4.
[23] J.-S. Hong and M. J. Lancaster, *Microstrip Filters for RF/Microwave Applications*. New York, NY, USA: Wiley, 2001.
[24] B. Lee, S. Nam, B. Koh, C. Kwak, and J. Lee, "K-band frequency tunable substrate-integrated-waveguide resonator filter with enhanced stopband attenuation," *IEEE Trans. Microw. Theory Techn.*, vol. 63, no. 11, pp. 3632–3640, Nov. 2015.

TAE-HAK LEE received the B.E. degree in electrical engineering from Konkuk University, Seoul, South Korea, in 2007, and the Ph.D. degree in radio communication engineering from Korea University, Seoul, in 2015. In 2015, he joined the Research Institute of Computer Information and Communication, Korea University. In 2016, he joined the École Polytechnique de Montréal, Montreal, QC, Canada, as a Postdoctoral Researcher. His current research interests include reconfigurable/tunable RF and microwave components, and RF energy harvesting. He was a recipient of the Postdoctoral Research Fellowship from the National Research Foundation.

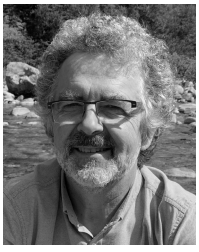

JEAN-JACQUES LAURIN (Senior Member, IEEE) received the B.Eng. degree in engineering physics from the Ecole Polytechnique de Montreal, Montreal, QC, Canada, and the M.A.Sc. and Ph.D. degrees in electrical engineering from the University of Toronto, Toronto, ON, Canada, in 1983, 1986, and 1991, respectively. In 1991, he joined the Poly-Grames Research Centre, Ecole Polytechnique de Montreal, where he is currently a Professor. He is the Co-Director of Center for Systems, Technologies, and Applications for Radiofrequency and Communications (STARaCom), a strategic research cluster in the province of Quebec. His research interests include antenna design and modeling, wave processing surfaces, near-field antenna measurement techniques, and electromagnetic compatibility.

KE WU (Fellow, IEEE) received the B.Sc. degree (Hons.) in radio engineering from Southeast University, Nanjing, China, in 1982, the D.E.A. degree (Hons.) in optics, optoelectronics, and microwave engineering from the Institut National Polytechnique de Grenoble (INPG), Gernoble, France, in 1984, and the Ph.D. degree (Hons.) in optics, optoelectronics, and microwave engineering from the University of Grenoble, Grenoble, in 1987. He was the Founding Director of the Center for Radiofrequency Electronics Research of Quebec (Regroupement stratégique of FRQNT) and the Tier-I Canada Research Chair in RF and Millimeter-Wave Engineering. He has been the Director of the Poly-Grames Research Center, Montreal. He is currently a Professor of electrical engineering and the NSERC-Huawei Industrial Research Chair of Future Wireless Technologies with Polytechnique Montréal, University of Montreal, Montreal, QC, Canada, and also with the School of Information Science and Engineering, Ningbo University, Ningbo, China, on leave from his home institution, leading a special 5G and future wireless research program. He has held guest, visiting, and honorary professorships with many universities around the world. He has authored or coauthored over 1200 refereed articles and a number of books/book chapters. He holds 50 patents. His current research interests include substrate-integrated circuits and systems, antenna arrays, field theory and joint field/circuit modeling, ultrafast interconnects, wireless power transmission and harvesting, megahertz-through-terahertz technologies, transceivers for wireless sensors and systems, as well as biomedical applications, and the modeling and design of microwave and terahertz photonic circuits and systems. He is a Fellow of the Canadian Academy of Engineering (CAE) and the Royal Society of Canada (The Canadian Academy of the Sciences and Humanities). He is also a member of Electromagnetics Academy, Sigma Xi, URSI, and IEEE-Eta Kappa Nu (IEEE-HKN). He was a recipient of many awards and prizes, including the first IEEE MTT-S Outstanding Young Engineer Award, the 2004 Fessenden Medal of the IEEE Canada, the 2009 Thomas W. Eadie Medal of the Royal Society of Canada, the Queen Elizabeth II Diamond Jubilee Medal, in 2013, the 2013 FCCP Education Foundation Award of Merit, the 2014 IEEE MTT-S Microwave Application Award, the 2014 Marie-Victorin Prize (Prix du Quebec—the Highest Distinction of Québec in the natural sciences and engineering), the 2015 Prix d'Excellence en Recherche et Innovation of Polytechnique Montréal, and the 2015 IEEE Montreal Section Gold Medal of Achievement. He has held key positions in and has served on various panels and international committees, including the Chair of Technical Program Committees, International Steering Committees, and International conferences/symposia. He served on the Editorial/Review Boards of many technical journals, transactions, proceedings, and letters, as well as scientific encyclopedia, including as the Editor and the Guest Editor of the IEEE MTT-S and Administrative Committee (AdCom), and as the Chair of the IEEE MTT-S Transnational Committee, the Member and Geographic Activities (MGA) Committee, the Technical Coordinating Committee (TCC), and the 2016 IEEE MTT-S President among many other AdCom functions. He was the General Chair of the 2012 IEEE Microwave Theory and Techniques (IEEE MTT-S) and International Microwave Symposium (IMS). He was the Chair of the joint IEEE Montreal Chapters of MTT-S/AP-S/LEOS and then the restructured IEEE MTT-S Montreal Chapter, Canada. He is the Chair of the IEEE MTT-S Inter Society Committee. He is the Inaugural Representative of North America as a member of the European Microwave Association (EuMA) General Assembly.